



## Engineered peptide-drug conjugate provides sustained protection of retinal ganglion cells with topical administration in rats

Henry T. Hsueh <sup>a,b,1</sup>, Renee Ti Chou <sup>c,1</sup>, Usha Rai <sup>a,d</sup>, Patricia Kolodziejski <sup>a,b</sup>, Wathsala Liyanage <sup>a,d</sup>, Jahnavi Pejavar <sup>a,b</sup>, Ann Mozzer <sup>a,d</sup>, Charlotte Davison <sup>a,b</sup>, Matthew B. Appell <sup>a,e</sup>, Yoo Chun Kim <sup>a,d</sup>, Kirby T. Leo <sup>a,f</sup>, HyeYoung Kwon <sup>a,b</sup>, Maanasa Sista <sup>a,g</sup>, Nicole M. Anders <sup>h</sup>, Avelina Hemingway <sup>h</sup>, Sri Vishnu Kiran Rompiccharla <sup>a,d</sup>, Ian Pitha <sup>a,d</sup>, Donald J. Zack <sup>a,d,i</sup>, Justin Hanes <sup>a,b,d,e,f,h</sup>, Michael P. Cummings <sup>c</sup>, Laura M. Ensign <sup>a,b,d,e,f,h,\*</sup>

<sup>a</sup> Center for Nanomedicine at the Wilmer Eye Institute, Johns Hopkins University School of Medicine, Baltimore, MD, USA

<sup>b</sup> Department of Chemical & Biomolecular Engineering, Johns Hopkins University, Baltimore, MD, USA

<sup>c</sup> Center for Bioinformatics and Computational Biology, University of Maryland, College Park, College Park, MD, USA

<sup>d</sup> Department of Ophthalmology, Johns Hopkins University School of Medicine, Baltimore, MD, USA

<sup>e</sup> Department of Pharmacology and Molecular Sciences, Johns Hopkins University, Baltimore, MD, USA

<sup>f</sup> Department of Biomedical Engineering, Johns Hopkins University, Baltimore, MD, USA

<sup>g</sup> Department of Biomedical Engineering, Case Western Reserve University, Cleveland, OH, USA

<sup>h</sup> The Sidney Kimmel Comprehensive Cancer Center at Johns Hopkins University, Baltimore, MD, USA

<sup>i</sup> Departments of Neuroscience, Molecular Biology and Genetics, and Genetic Medicine, Johns Hopkins University School of Medicine, Baltimore, MD, USA

### ABSTRACT

Effective eye drop delivery systems for treating diseases of the posterior segment have yet to be clinically validated. Further, adherence to eye drop regimens is often problematic due to the difficulty and inconvenience of repetitive dosing. Here, we describe a strategy for topically dosing a peptide-drug conjugate to achieve effective and sustained therapeutic sunitinib concentrations to protect retinal ganglion cells (RGCs) in a rat model of optic nerve injury. We combined two promising delivery technologies, namely, a hypotonic gel-forming eye drop delivery system, and an engineered melanin binding and cell-penetrating peptide that sustains intraocular drug residence time. We found that once daily topical dosing of HR97-SunitiGel provided up to 2 weeks of neuroprotection after the last dose, effectively doubling the therapeutic window observed with SunitiGel. For chronic ocular diseases affecting the posterior segment, the convenience of an eye drop combined with intermittent dosing frequency could result in greater patient adherence, and thus, improved disease management.

### 1. Introduction

Achieving drug delivery to the retina with topical eye drops is a “holy grail” of ocular drug delivery. Unfortunately, precorneal clearance, ocular tissue barriers such as the cornea and sclera, and uveal clearance reduce the amount and duration of drug delivery to posterior segment cells and tissues. Thus, there are no FDA approved eyedrops for treating diseases of the posterior segment, and patient adherence to many eye drops is limited by the necessity of dosing multiple times per day [1,2]. To overcome these challenges, a drug delivery system that provides longer corneal residence time and increased intraocular absorption could facilitate increased drug delivery to the retina. In addition, increasing intraocular drug retention time could further improve drug

accumulation and sustain the duration within the therapeutic window.

We recently described the development of a hypotonic, thermosensitive gel-forming eye drop that provided increased and sustained intraocular drug absorption without increased systemic drug exposure [3]. In addition, we described that sunitinib, a dual leucine zipper kinase (DLK) and leucine zipper kinase (LZK) inhibitor that promotes retinal ganglion cell (RGC) survival, could be effectively delivered to the posterior segment using the gel-forming eye drop [4–6]. The combination of enhanced intraocular absorption provided by the gel-forming eye drop (SunitiGel) and the intrinsic melanin binding properties of sunitinib led to significant protection of RGCs with only once weekly eye drop dosing [6]. Studies have shown that ocular melanin could affect drug distribution and retention in ocular pigmented cells [7], and prolong the

\* Corresponding author at: Center for Nanomedicine at the Wilmer Eye Institute, Johns Hopkins University School of Medicine, Baltimore, MD, USA.

E-mail address: [lensign@jhmi.edu](mailto:lensign@jhmi.edu) (L.M. Ensign).

<sup>1</sup> Equally contributing authors.



effects of certain drugs [8]. Machine learning models have also been developed to predict the melanin binding potential of small molecule ophthalmic drugs [9]. We recently described an approach for applying machine learning to engineer multifunctional peptide adaptors to embody high melanin binding, cell-penetration, and low cytotoxicity in the same peptide sequence [10]. The highest performing peptide, HR97, was conjugated to the intraocular pressure (IOP) lowering drug brimonidine tartrate, to impart these properties to the peptide-drug conjugate. We demonstrated that a single intracameral injection of the HR97-brimonidine conjugate provided a larger IOP reduction in normotensive rabbits that lasted for up to 18 days, which was significantly longer than injection of brimonidine alone (7 days), or topical brimonidine tartrate eye drops (Alphagan®, 8 h). Accumulation of the HR97-brimonidine conjugate in the melanin containing cells of the iris likely contributed to the magnitude and duration of the therapeutic effect in the anterior segment.

In this work, we hypothesized that conjugation of the engineered multifunctional peptide adaptors to sunitinib for delivery to the posterior segment using the gel-forming eye drop would provide even more prolong therapeutic effects in the posterior tissues. We observed that the HR97-sunitinib conjugate had increased binding capacity to ocular melanin and was cleaved by proteases to release free sunitinib *in vitro*. Rats were dosed topically with HR97-SunitiGel once daily for seven days, followed by optic nerve head crush at various times after the last dose to assess the duration of RGC protection. We observed that the HR97-SunitiGel showed prolonged neuroprotective effects for up to 2 weeks after the last topical dose, whereas the protective effect of SunitiGel was only observed at 1 week after the last dose. Our observations support the potential for improving and prolonging therapeutic delivery to the posterior segment tissues by addressing multiple barriers to drug delivery and retention in the eye.

## 2. Materials and methods

### 2.1. Material sources

Sunitinib base and sunitinib malate were purchased from LC laboratories (Woburn, MA, USA). Eumelanin from *Sepia officinalis*, 0.22 µm Millex-GV PVDF filter, ferric ammonium citrate, bovine serum albumin (BSA), Tween 20, fetal bovine serum (FBS), trifluoroacetic acid (TFA), tert-Butyl methyl ether (MTBE), thionyl chloride, tetrabutylammonium iodide, N,N-diisopropylethylamine, human cathepsins B, K, L, and S, Whatman® Anstop® 0.02 µm syringe filter, Poloxamer 407, and Triton X-100 were purchased from Sigma Aldrich (St. Louis, MO, USA). ARPE-19 cells (CRL-2302) and DMEM:F12 medium were purchased from the American Type Culture Collection (Manassas, VA, USA). Rapid equilibrium dialysis (RED) 8 K device, DMEM with high glucose and pyruvate, Trypsin-EDTA (0.25% w/v) with phenol, RIPA lysis buffer, RNA binding protein, mRNA processing factor (RBPMs) rabbit anti rat polyclonal antibody, Alexa Fluor 555 conjugated goat anti-rabbit IgG (H + L) secondary antibody, penicillin/streptomycin, 4',6-diamidino-2-phenylindole, dihydrochloride (DAPI), Fluoromount-G, Image-iT™ Fixative Solution (4% w/v formaldehyde, methanol-free), and penicillin/streptomycin were purchased from Thermo Fisher Scientific (Waltham, MA, USA). Disposable PD-10 desalting columns were purchased from VWR (Radnor, PA, USA). Dulbecco's Phosphate Buffered Saline (DPBS), 1 × phosphate buffered saline (PBS), 10 × PBS, high-performance liquid chromatography (HPLC) grade acetonitrile (ACN), dimethylformamide (DMF), and water were purchased from Fisher Scientific (Hampton, NH, USA). Mc-Val-Cit-PAB was purchased from Cayman Chemical (Ann Arbor, MI, USA). Endotoxin-free ultra-pure water was purchased from Millipore Sigma (Burlington, MA, USA). Isoflurane was purchased from Baxter (Deerfield, IL, USA). Reverse-action forceps were purchased from World Precision Instruments (Sarasota, FL, USA). Neomycin, polymyxin b, and bacitracin zinc ophthalmic ointment were purchased from Akorn (Lake Forest, IL, USA).

### 2.2. Traceless linker system for conjugating HR97 to sunitinib

The traceless linker system was designed for the release of intact parent drug when triggered by an intracellular chemical and enzymatic event, such as protease cleavage of the amide bond [11]. Activation of the linker, MC-Val-Cit-PAB-OH (maleimidocaproyl-L-valine-L-citrulline-p-aminobenzyl alcohol), was conducted as previously described with minor modifications [10,11]. MC-Val-Cit-PAB-OH (8.68 g, 15.2 mmol) was suspended in DMF (43.4 mL) at 0 °C with water bath sonication for 30 min. After solids were fully dispersed, thionyl chloride (1.22 mL, 16.7 mmol) was added dropwise. Following the addition, the reaction was held at 0 °C for 45 min and then treated slowly with water (130 mL) to precipitate a yellow solid (MC-Val-Cit-PAB-Cl), which was collected by filtration. The solid was washed sequentially with water and MTBE and dried under vacuum (~30% yield) [11]. Sunitinib base was combined with MC-Val-Cit-PAB-Cl (1.1 eq) in DMF (0.25 M) at room temperature. Tetrabutylammonium iodide (0.5 eq) was added to the solution, followed by the addition of N,N-diisopropylethylamine (2.5 eq), and the mixture was stirred for 24 h. The mixture was diluted with 50:50 acetonitrile:water at 40-fold dilution for purifying MC-Val-Cit-PAB-sunitinib. A Shimadzu LC20 HPLC system coupled with the photodiode array detector (PDA) and the Phenomenex reverse-phase preparative HPLC column (Gemini® 10 µm C18 110 Å, LC Column 250 × 21.2 mm, AXIA™ Packed) was used to separate and collect the peptide-drug conjugates with an elution gradient of 10/90/90/10% v/v solvent B (TFA 0.05% v/v in can) at 1/11/13/15 min with a flow rate of 10 mL/min. The collected fractions were then transferred to the 20 mL scintillation vials and a Biotage V-10 solvent evaporator with volatile mode was used to remove ACN. The solution fractions were frozen and lyophilized (~7% yield). Nuclear magnetic resonance (NMR) spectroscopy was used to confirm the presence of key functional groups in the products at each stage of the synthesis, including sunitinib base, Mc-VC-PAB-Cl, and Mc-VC-PAB-sunitinib. All compounds were dissolved in deuterated DMSO and characterized with a Bruker spectrometer (500 MHz). <sup>1</sup>H chemical shifts were reported in ppm ( $\delta$ ) and the DMSO peak was used as an internal standard. Data were processed using TopSpin NMR Data Analysis software, version 4.1.0, from Bruker. HR97 with cysteine at the C-terminus as the functional group for linker conjugation (FSGKRRKRKPRC, MW 1.5 kDa, >97% purity from Thermo Fisher peptide custom service) was conjugated to the quaternary-ammonium-linked sunitinib (MC-Val-Cit-PAB-sunitinib) via a thiol-maleimide reaction. The MC-Val-Cit-PAB-sunitinib was first dissolved in 1 mL of PBS at 5 mg/mL, and the HR97 peptide powder (0.5 eq) was added. The solution mixture was adjusted to pH 7.4 and allowed to react for 2 h at room temperature. The solution was then added to 1 mL of acetonitrile and purified with the same prep-HPLC conditions. The collected fractions were transferred to 20 mL scintillation vials and a Biotage V-10 solvent evaporator with volatile mode was used to remove ACN. The solutions were lyophilized and stored at -20 °C (~29% yield). For the sample preparation and MALDI-TOF analysis, the MALDI matrix sinapic acid (10 mg) was dissolved in 1 mL of acetonitrile in water (1:1) with 0.1% TFA, and 1 µL of sample (50 µM) was deposited on the MALDI sample plate. The matrix (2 µL, 10 mg/mL) was deposited on the air-dried sample and allowed to air dry for 10–20 min. The MALDI-TOF MS analysis was performed on a Bruker Voyager DE-STR MALDI-TOF (Mass Spectrometric and Proteomics core, Johns Hopkins University, School of Medicine) operated in linear, reflective-positive ion mode.

### 2.3. In vitro stability test for HR97-sunitinib conjugate

Two pairs of human donor eyes were obtained from the Lions Gift of Sight under protocol IRB00056984 approved by the Johns Hopkins University School of Medicine Institutional Review Board. Both donors were male with a mean age of 74.5. The post-mortem times ranged from 35 to 40 h. The eyes were kept at 4 °C during transport and arrived within 48 h post-mortem. The vitreous from each eye was isolated,

combined, and filtered through a 0.02 µm syringe filter to remove cell debris. The aqueous was similarly combined and filtered. Each fluid type was aliquoted into 3 replicates (700 µL) and HR97-sunitinib (1 mg/mL) was added, and the mixture was incubated at 37 °C ( $n = 3$ ). On day 0, 1, 7, 14, 21, and 28, 100 µL of the supernatant was collected, diluted with 900 µL of ACN, and characterized by HPLC (Prominence LC2030, Shimadzu) with Luna® 5 µm C18(2) 100 Å LC column 250 × 4.6 mm (Phenomenex, Torrance, CA). Separation was achieved with a Luna® 5 µm C18(2) 100 Å LC column 250 × 4.6 mm (Phenomenex) at 40 °C using isocratic flow (1 mL/min 60% TFA 0.1% in ACN). HR97-sunitinib was detected at  $\lambda_{max} = 420$  nm (HR97-sunitinib retention time = 1.9 min). The area under the curve (AUC) at day 0 was used to normalize the AUCs calculated at days 1, 7, 14, 21, and 28.

#### 2.4. Cathepsin cleavage assay for HR97-sunitinib conjugate

An assay to demonstrate enzymatic cleavage of the linker was used as previously described with adaptations [10,11]. In brief, the HR97-sunitinib conjugate solution (200 µM) was diluted with an equal volume of 100 mM citrate buffer at pH 5.5. Cysteine was added to a final concentration of 5 mM before the addition of human cathepsins B, K, L, and S (150 nM each). The mixture was then incubated from 0 h (control group) to 48 h at 37 °C. The solutions were further diluted with ACN to 1 mL and the conjugate concentration was measured using the HPLC method described above. The concentration of HR97-sunitinib at 0 h was used to normalize the ratio remaining at later time points.

#### 2.5. In vitro melanin binding assay

Melanin nanoparticles (mNPs) were synthesized from the eumelanin of *Sepia officinalis* as previously described [10]. In brief, 10 mg/mL of eumelanin was suspended in DPBS using an ultrasonic probe sonicator (Sonics, Vibra Cell VCX-750 with model CV334 probe, Newtown, CT, USA) by pulsing 1 s on/off at 40% amplitude for 30 min in a 4 °C water bath. The suspension was then filtered through a 0.22 µm Millex-GV PVDF filter and transferred to PD-10 desalting columns. The resulting mNPs solution was lyophilized for 7 days and stored at –20 °C until further use. Sunitinib malate and HR97-sunitinib at a range of concentrations (12.5, 25, 50, 100 µg/mL) were dissolved in pH 6.5 PBS solution in 3 replicates. The solutions (400 µL) were then mixed thoroughly with 400 µL of 1 mg/mL mNPs in pH 6.5 PBS solution and transferred to the inner reservoir of the rapid equilibrium dialysis (RED) device inserts (8 K MWCO). The outer reservoir was filled with 800 µL of pH 6.5 PBS solution. The samples were incubated on an orbital shaker with temperature controlled at 37 °C and 300 rpm for 48 h. The solutions from outer reservoir (free drug) were then collected and transferred to an autosampler vial for HPLC analysis (Prominence LC2030, Shimadzu, Columbia, MD) with the photodiode-array detection (PDA) system. Separation was achieved with a Luna® 5 µm C18(2) 100 Å LC column 250 × 4.6 mm (Phenomenex, Torrance, CA) at 40 °C using isocratic flow. The amount of bound drug was used to calculate the binding capacity (moles drug/mg melanin) and the dissociation constant ( $K_d$ ) as previously described [6,12]. The data point of HR97 conjugated to biotin for the high-throughput melanin binding screening assay was originally shown in our previous work [10].

#### 2.6. In vitro cell uptake assay

The ARPE-19 cells and the induction of melanin expression in ARPE-19 cells were cultured as previously described [6]. One million ARPE-19 cells cultured for 2 months were collected for each condition and plated in 6-well plates for another 48 h. Sunitinib malate and HR97-sunitinib (25 µg/mL equivalent of sunitinib) in PBS were added to the cells for 6 h at 37 °C. The cells were then washed for 3 times with PBS using centrifugation at 3000 rcf for 5 min. After the last wash, the cells were incubated in acetonitrile at room temperature for 24 h to extract the

drug. The samples were then centrifuged at 17,000 rcf at 37 °C for 30 min, and the supernatant was collected to measure the drug concentration using HPLC as described above.

#### 2.7. Characterization of drug solubility

To measure solubility, 1 mg of sunitinib malate, sunitinib base, or HR97-sunitinib was placed in microcentrifuge tubes with 0.2 mL of PBS. The samples were then placed on an orbital shaker (150 rpm) in an incubator at 37 °C. After 7 days, samples were collected and centrifuged at 17,000 rcf for 30 min. The supernatants were collected, and concentrations were measured using HPLC as described above for sunitinib. Supernatant samples were mixed 1:10 with ACN containing 0.1% v/v TFA. ACN and water were used as a mobile phase at a ratio of 55:45. Samples were eluted isocratically at a flow rate of 1 mL/min through a C18-reversed phase column at 40 °C. UV absorbance was monitored at 420 nm.

#### 2.8. Animal studies — Animal welfare statement

All experimental protocols were approved by the Johns Hopkins Animal Care and Use Committee. All animals were handled and treated in accordance with the Association for Research in Vision and Ophthalmology Statement for Use of Animals in Ophthalmic and Vision Research. Equivalent numbers of both male and female animals were used. Brown Norway rats (6–10 weeks) were obtained from Harlan/Envigo. Dutch Belted rabbits (4–5 mo) were obtained from Robinson Services, Inc.

#### 2.9. Rat optic nerve head (ONH) crush model

We previously described that the delivery of sunitinib malate in SunitiGel provided sustained RGC protection with once weekly dosing in an optic nerve head (ONH) crush model [6]. The model was implemented similarly to investigate the timing of quantification of RGCs in the time-course study and the potential benefit of the HR97 peptide conjugation. In the time-course study, Brown Norway rats received the optic nerve head crush on day 0, and on day 1, 4, 7, 11, 14, or 19, the retinas were harvested and stained with DAPI and RBPMS for quantifying the remaining RGCs using the AI deep learning algorithm ( $n = 6$ ). In the HR97-SunitiGel RGC protection study, Brown Norway rats ( $n = 36$ , split into 3 groups of 12) received seven daily doses (5 µL) of 1 mg/mL sunitinib equivalent in HR97-SunitiGel (6.2 mg of HR97-sunitinib dissolved in 1 mL of 12% w/w F127). The ONH crush procedure was then performed on separate groups of animals on day 0, 7, and 14 after the last dose. Another group of rats ( $n = 12$ ) received seven daily eye drops (5 µL) of water as a sham control prior to undergoing the ONH crush procedure on day 0 (immediately after the last dose). The third group of rats ( $n = 12$ ) received seven daily eye drops (5 µL) of 1 mg/mL equivalent sunitinib in SunitiGel (1.34 mg sunitinib malate in 1 mL of 12% w/w F127, equal to 1 mg/mL sunitinib equivalent). Rats received general anesthesia prior to topical anesthesia. Proparacaine hydrochloride (0.5% w/v) was applied topically to the right eye 1 min before the surgical process. The temporal conjunctiva of the left eye was grasped with 0.12 mm toothed forceps and incised parallel to the limbus with sharp iris scissors. The dissection was performed using two pairs of curved blunt-tipped forceps, and the orbital fat and soft tissue were retracted to expose the orbital portion of the optic nerve. The optic nerve was crushed at a position 1.5–2 mm posterior to the globe using reverse-action forceps for 10 s. The orbital soft tissue was then repositioned over the nerve and the conjunctiva was left to close by secondary intention [6]. After the procedure, topical bacitracin-neomycin-polymyxin ophthalmic ointment was applied to both eyes to prevent infection. Any animals that bled severely during the surgery were sacrificed and excluded from the study. Seven days after the optic nerve crush, rats were sacrificed for subsequent analyses.

## 2.10. Retinal ganglion cell staining and imaging

The process of harvesting retina tissues, staining, and imaging were performed as previously described [6,13]. Rats were sacrificed by cervical dislocation under general anesthesia. The eyes were then harvested and fixed with 4% w/v paraformaldehyde for 2 h. The retinas were removed, incised for flat mounting, and post-fixed for 2 h. The retinas were then washed with PBS containing 0.5% w/v Triton-100 for 30 min and incubated for 3 days at 4 °C in a solution containing rabbit anti-rat RBPMS antibody diluted 1:250 in PBS with 1% w/v Triton X-100 and 1% w/v BSA. The retinas were then washed for three times with PBS containing 0.5% w/v Triton-100 and incubated overnight at 4 °C in a solution containing Goat anti-Rabbit IgG H&L Secondary Antibody Alexa Fluor 555 (Thermo Fisher, Waltham, MA, USA) diluted 1:1000 in PBS with 1% w/v Triton X-100 and 1% w/v BSA. The retinas were washed again for three times and incubated overnight in DAPI diluted 1:1000 in PBS. The resulting retinal wholemount was then mounted on a slide using Fluoromount-G. The prepared retinas were imaged with a Zeiss 710 Confocal Microscope. For each retinal wholemount, 16 images were taken from the region 2–3 mm from the optic nerve per each retinal quadrants using a 40× objective. The DAPI images were pseudo-colored in blue and the RBPMS images were pseudo-colored in red.

## 2.11. Retinal ganglion cell counting

For training the TensorFlow Object Detection model (TensorFlow Version 1.2), 173 images containing 4247 RGCs, and 62 images containing 1757 RGCs were manually labeled using the *LabelImg* function as the training and testing sets, respectively. Faster R-CNN with Inception Resnet v2 and SSD-MobileNet were used as the TensorFlow Object Detection models. The weighted sigmoid (sigmoid cross-entropy loss function) was used for the classification loss, and the weighted smooth L1 (box regression in object detection) was used for the localization loss. To avoid overfitting, the training process was terminated when the total loss was <1 or when the total loss has reached a steady state. An inference graph at each epoch was created with the script *export\_inference\_graph.py* provided in the *object\_detection* directory. The CellProfiler, version 3.1.9, with CellProfiler Analyst, version 2.2.1, was used in this study. The *Metadata* function was used to extract the DAPI and RBPMS sub-layer information from confocal images and the names were assigned using *NamesAndTypes*. The DAPI layers were first smoothed with the Gaussian filter function, and the *IdentifyPrimaryObjects* function was used to identify the DAPI areas using global and three-class Otsu threshold methods. The RBPMS sub-layers were smoothed with the Guassian Filter and then again smoothed with the Median Filter because the RBPMS staining with the RGCs had given uneven intensities and confused the program in the subsequent steps. The *IdentifySecondaryObjects* function with Propagation strategy and adaptive, three-class Otsu, and foreground methods were used to identify the RBPMS as secondary objects based on the DAPI areas identified in the primary object session. The object shape size, object intensity, and texture were measured for both DAPI and RBPMS objects as the features for CellProfiler Analyst, version 2.2.1. An SQLite database was generated after the CellProfiler had finished the feature extraction. In CellProfiler Analyst, *RandomForestClassifier* was used and RGCs in the unclassified window were dragged to the positive area following the suggested protocols. >100 cells in each positive and negative class were then manually assigned until the classification accuracy reached over than 90% computed using the evaluation function. Finally, the output scores were used to quantify the RGCs in each image. RGCs in another set of 200 images were manually counted by three researchers masked to the sample identity and the means were calculated for each image. In a rare instance that the cell count per image varied by >10%, the images were recounted by each person until the variance was <10%. Quantification results of the RGC images predicted by Faster R-CNN with Inception Resnet v2, SSD-MobileNet, and Cell Profiler Analyst models

were compared to the manual counting results using Pearson correlation.

## 2.12. Pharmacokinetic studies

Brown Norway rats ( $n = 6$ ) received once daily eye drops (5 µL) containing 1 mg/mL sunitinib equivalent in HR97-SunitiGel (6.2 mg of HR97-sunitinib dissolved in 1 mL of 12% w/w F127) or containing 1 mg/mL equivalent sunitinib in SunitiGel (1.34 mg sunitinib malate in 1 mL of 12% w/w F127, which was equal to 1 mg/mL sunitinib equivalent) for seven days. Fourteen days after the last dose, the iris, choroid, and retina were collected and analyzed for sunitinib concentration using LC-MS/MS. Similarly, Dutch Belted rabbits ( $n = 4$ ) received once daily eye drops (50 µL) containing 1 mg/mL sunitinib equivalent in HR97-SunitiGel or containing 1 mg/mL equivalent sunitinib in SunitiGel. Two hours after the last dose, the iris, choroid, and retina were collected for analysis of sunitinib concentration using LC-MS/MS.

## 2.13. Measurement of sunitinib in ocular tissues

Sunitinib concentrations in ocular tissues were measured by liquid chromatography-tandem mass spectrometry (LC-MS/MS) as previously described [3]. All samples were collected in pre-weighed tubes and stored at –80 °C until being processed for analysis. Tissue samples were homogenized in 100–600 µL 1 × PBS using a Next Advance Bullet Blender before extraction. Sunitinib was extracted from 15 to 50 µL of tissue homogenates with 50 µL of acetonitrile containing 50/50/2.5 ng/mL of the internal standards (sunitinib-d10). The top layer was then transferred to an autosampler vial for LC-MS/MS analysis after centrifugation. All ocular tissue samples were analyzed using a 1 × PBS standard curve for sunitinib. Separation was achieved with Waters Cortecs C18 (2.1 × 50 mm, 2.7 µm). The column effluent was monitored using a Sciex triple quadrupol 4500 with electrospray ionization operating in the positive mode. The Mobile phase A was water containing 0.1% formic acid and the mobile phase B was acetonitrile containing 0.1% formic acid. The gradient started with the mobile phase B held at 10% for 0.5 min and increased to 100% within 0.5 min; 100% of mobile phase B was held for 1 min, and then the mobile phase B returned back to 10% and was allowed to equilibrate for 1 min. The total run time was 3 min with a flow rate of 0.3 mL/min. The spectrometer was programmed to monitor the following MRM transition 399.1 → 283.2 for sunitinib and 409.1 → 283.2 for the internal standard, sunitinib-d10. Calibration curve for sunitinib was computed using the area ratio peak of the analysis to the internal standard by using a quadratic equation with a x<sup>2</sup> weighting function over the range of 0.25–500, with dilutions up to 1:100 (v:v). Core technicians performing sample and data analysis were masked to the treatment groups.

## 2.14. Statistical analyses

Statistical analyses of two groups were conducted using two-tailed Student's *t*-test, two-tailed Mann–Whitney test, or two-way analysis of variance (ANOVA). For comparison of multiple groups, one-way ANOVA with Dunnett's multiple comparison test was used. Pearson correlation coefficients (*r*) and the corresponding *p*-values (two-tailed) were calculated to assess the relationships between model predictions and the mean values of the manual counting.

## 3. Results

### 3.1. Conjugation of HR97 peptide to sunitinib increases melanin binding *in vitro*

We developed a scheme for conjugating HR97 to sunitinib via a quaternary-ammonium traceless linker system and structurally confirmed each intermediate product by NMR, HPLC, and MALDI-TOF

**(Supplementary Figs. 1–5).** When incubated in human vitreous and aqueous fluids *ex vivo* for 28 days, only ~15% (Fig. 1A) and ~5% (Fig. 1B) of the sunitinib were released. In contrast, upon incubation with supraphysiological concentrations of human cathepsins to enzymatically cleave the linker, ~72% of the sunitinib was released within 48 h (Fig. 1C, Supplementary Fig. 6). The conjugation of HR97 to sunitinib increased the solubility to 56-fold compared to sunitinib base and 5.5-fold compared to sunitinib malate (Fig. 1D). Although sunitinib already shows relatively high intrinsic melanin binding properties compared to other ophthalmic drugs, conjugation to HR97 provided a 1.3-fold increase in melanin binding capacity compared to sunitinib *in vivo* ( $K_d$   $7.30 \times 10^{-6}$  M vs.  $5.51 \times 10^{-6}$  M) (Fig. 2A). Additionally, HR97-sunitinib provided a 2.2-fold increase in cell uptake compared to sunitinib in non-induced ARPE-19 cells (Fig. 2B). When incubated with ARPE-19 cells induced to produce melanin, HR97-sunitinib provided a 1.4-fold increase in cell uptake compared to sunitinib (Fig. 2B).

### 3.2. A deep learning object detection model was more accurate in counting RGCs

A key aspect of assessing neuroprotective capacity involves counting RGCs in different regions of flat-mounted retina tissues. Manual cell counting can be time-consuming, so we sought to develop a reliable, automated image analysis method. We used RGC images to train SSD-MobileNet (Supplementary Fig. 7) and Faster R-CNN with Inception Resnet v2 (Supplementary Fig. 8) models, both of which are often used in the object detection research [14,15]. The Faster R-CNN with Inception Resnet v2 performed well in both high (> 60) and low (< 20) cell density image conditions ( $r = 0.993$ ), whereas the SSD-MobileNet slightly over-performed when the RGCs density was high in the images (Fig. 3A–B). The two object detection models were then compared to CellProfiler Analyst, a well-established open-source program for cell

classification and recognition. The prediction results generated by CellProfiler Analyst were more vulnerable to the quality of the images, with lower prediction accuracies for both high and low cell density images compared to the deep learning object detection models ( $r = 0.947$ ) (Fig. 3C). We further demonstrated the capability of Faster R-CNN inception Resnet v2 in identifying the RGCs in various RGCs image conditions, such as high and low cell density, oversaturated, and dim image settings (Fig. 3D–I). We used the trained Faster R-CNN with Inception Resnet v2 model (hereafter referred to as the cell counting program) to assess retinal images collected from a time-course study of the rat ONH crush animal model to identify the optimal screening window for a neuroprotection drug delivery study (Supplementary Fig. 9A). The quantification results using the cell counting program showed that the number of surviving RGCs decreased most rapidly between days 4 and 11 after the optic nerve head crush, and the curve started to flatten 11 days after the procedure (Supplementary Fig. 9B). Thus, a period of 7 days after the crush procedure was selected as the timeframe to assess RGC protection.

### 3.3. HR97-SunitiGel showed prolonged neuroprotective effects compared to SunitiGel

We next tested the potential duration of neuroprotection after topical dosing of HR97-SunitiGel. Brown Norway rats were dosed with HR97-SunitiGel or SunitiGel daily for 7 days, the optic nerve head crush procedure was performed on day 0, 7, or 21 after the last topical dose, and the RGC survival was characterized 7 days after the injury (Fig. 4A). The RGC quantification results computed by the cell counting program showed that the neuroprotective effect of HR97-SunitiGel lasted for at least 2 weeks after the last dose ( $869.2 \pm 58.86$  RGCs/mm<sup>2</sup> compared to sham,  $623.7 \pm 70.39$  RGCs/mm<sup>2</sup>, Fig. 4B), with the effect waning 4 weeks after the last dose ( $692.2 \pm 96.58$  RGCs/mm<sup>2</sup>, Fig. 4C). In

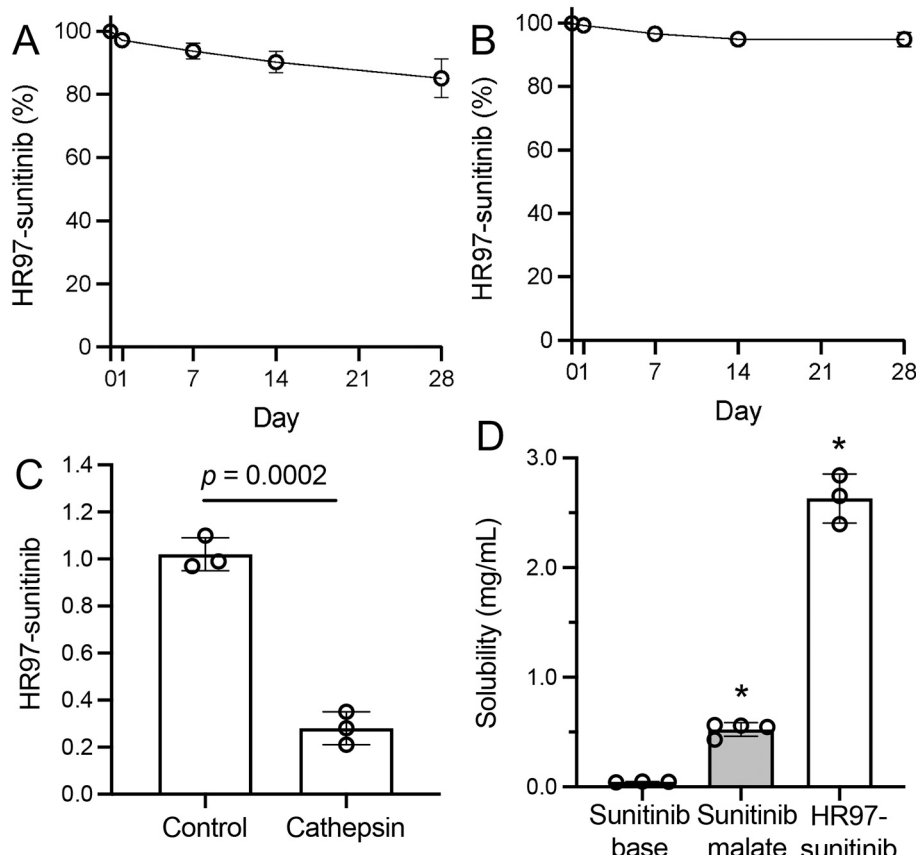


**Fig. 1.** Characterization of HR97-sunitinib stability and solubility. *In vitro* stability of HR97-sunitinib conjugate in (A) human vitreous and (B) human aqueous humor for 28 days. The amount of HR97-sunitinib remaining was normalized to the starting concentration ( $n = 3$ ). Data are presented as mean  $\pm$  SD. (C) Cathepsin cleavage assay of the HR97-sunitinib conjugate. HR97-sunitinib was incubated with human cathepsin cocktails (Cathepsin) or buffer only (Control) for 48 h at 37 °C ( $n = 3$ ). The amount of HR97-sunitinib remaining was normalized to the starting concentration ( $n = 3$ ). Data are presented as mean  $\pm$  SD,  $p$ -value = 0.0002. (D) Conjugation to HR97 increased the intrinsic solubility of sunitinib compared to sunitinib free base and sunitinib malate salt ( $n = 3$ ). Data are presented as mean  $\pm$  SD, \* $p$  < 0.01 compared to sunitinib base.

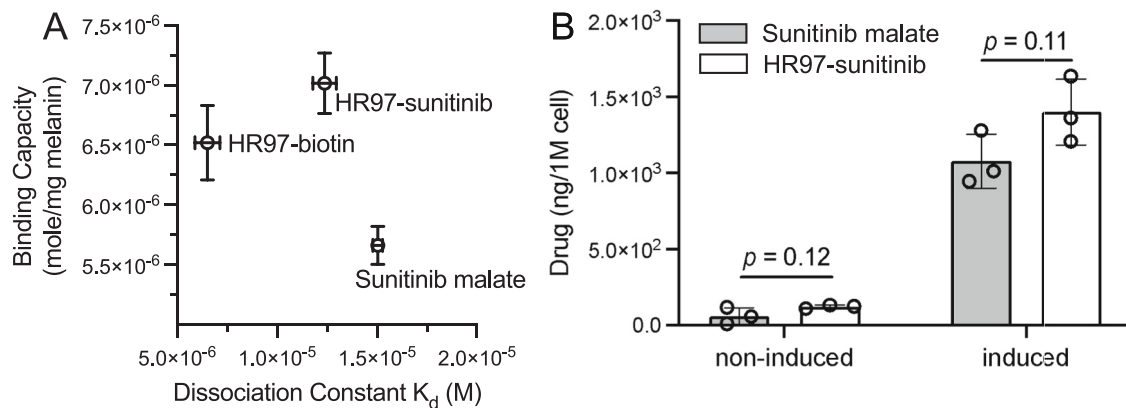


**Fig. 2.** Characterization of HR97-sunitinib melanin binding and cell uptake *in vitro*. (A) *In vitro* melanin binding capacity and dissociation constant of HR97-biotin [10], HR97-sunitinib, and sunitinib malate ( $n = 3$ ). Lower dissociation constant indicates stronger binding. Data are presented as mean  $\pm$  SD. (B) ARPE-19 cells were cultured under normal conditions (ARPE) or under conditions that induce melanin production (induced ARPE) and incubated with sunitinib malate or HR97-sunitinib for 6 h. The cells were then collected and washed prior to extracting sunitinib. Drug content was normalized to per 1 million cells. Data are shown as mean  $\pm$  SD,  $n = 3$ .

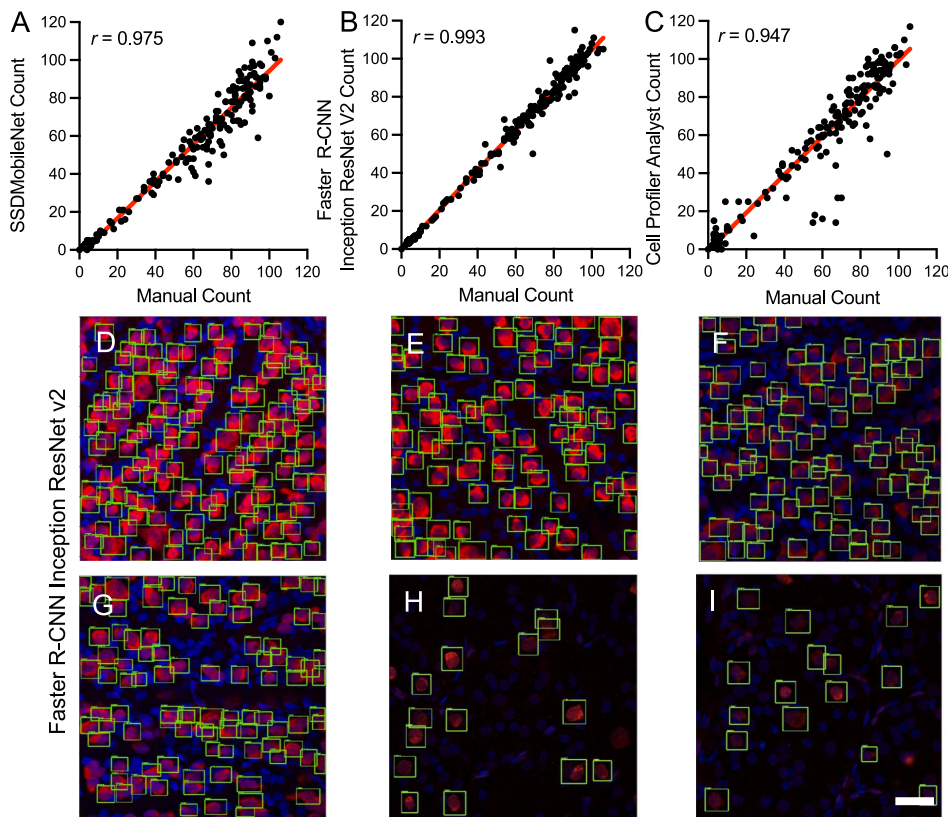


**Fig. 3.** Comparison between SSD-MobileNet, Faster R-CNN Inception ResNet v2, and CellProfiler software. A total of 173 images with 4247 manual labeled cells from both healthy and ONH crushed retinas were used to train the SSD-MobileNet and Faster R-CNN Inception ResNet v2 models. The same image sets were used as inputs to CellProfiler for generating the features. Simple linear correlations between automated and manual quantification of 200 RGCs  $40\times$  images were calculated and the Pearson correlation coefficient ( $r$ ) are noted. (A) SSD-MobileNet (epoch 51,350),  $r = 0.975$ , which is significant with the  $p$ -value threshold of 0.0001 (two-tailed). (B) Faster R-CNN Inception ResNet v2 (epoch 13,683),  $r = 0.993$ , which is significant with the  $p$ -value threshold of 0.0001 (two-tailed). (C) The random forest classifier was used in CellProfiler Analyst,  $r = 0.947$ , which is significant with the  $p$ -value threshold of 0.0001 (two-tailed). Among the three different platforms, the Faster R-CNN model more accurately quantified cells in images with (D) oversaturated and crowded RGCs; (E) mid-density RGCs; (F) low brightness RGCs; (G) mid-density, low brightness RGCs; (H) low density RGCs; and (I) low density, low brightness RGCs. Scale bar = 50  $\mu$ m.

contrast, SunitiGel provided significant RGC protection at 1 week ( $846.4 \pm 125.8$  RGCs/mm $^2$ ) compared to the sham group, with protection waning 2 weeks after the last dose ( $717.3 \pm 59.94$  RGCs/mm $^2$ , Fig. 4D).

#### 3.4. HR97-SunitiGel provided increased intraocular residence time in rats and therapeutically relevant drug delivery to the posterior segment in rabbits

Based on the improved efficacy of HR97-SunitiGel at the 2-week timepoint compared to SunitiGel, pharmacokinetic characterizations were conducted in rats to determine differences in intraocular drug concentrations. At week 2 after the last topical dose, HR97-SunitiGel

provided 52-fold (362.2 ng/g vs. 7.0 ng/g), 21-fold (2430.0 ng/g vs. 116.4 ng/g), and 1.3-fold (7824.6 ng/g vs. 6093.5 ng/g) higher concentrations of combined sunitinib and N-desethyl sunitinib in the rat retina, choroid/RPE, and iris/ciliary body, respectively, compared to SunitiGel (Fig. 5A). To subsequently confirm that therapeutically relevant drug concentrations could be achieved in the larger eyes, rabbits were dosed once daily for seven days with HR97-SunitiGel or SunitiGel. At 2 h after the last dose, HR97-SunitiGel provided 4.5-fold (27.8 ng/g vs. 6.1 ng/g), 4.7-fold (54.5 ng/g vs 11.5 ng/g), and 3.8-fold (182.8 ng/g vs 48.5 ng/g) higher concentrations of combined sunitinib and N-desethyl sunitinib in the rabbit retina, choroid, and iris, respectively, compared to SunitiGel (Fig. 5B). Importantly, the concentrations of

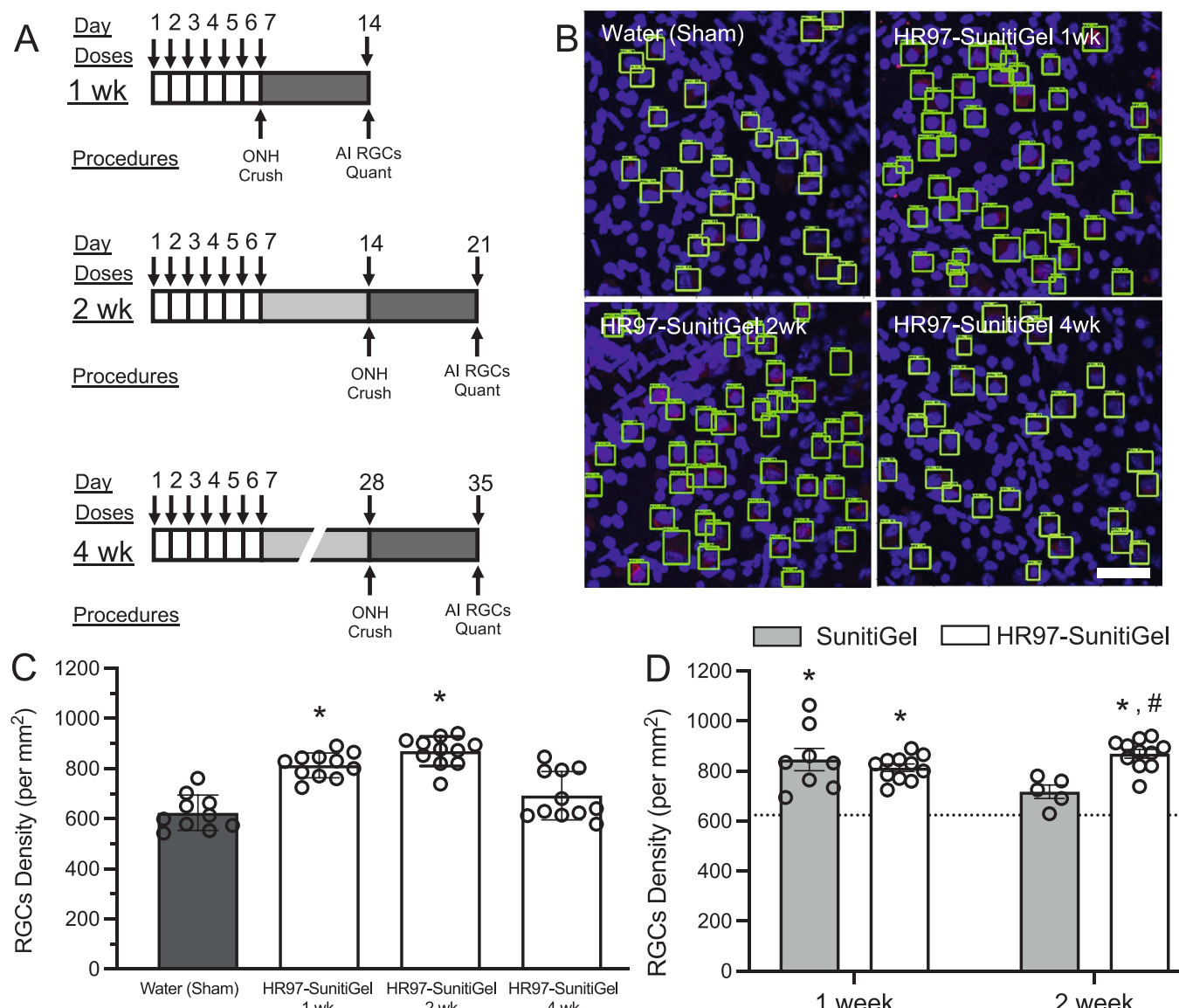


**Fig. 4.** HR97-SunitiGel extended RGC protection to at least 2 weeks after the last topical dose in rat model of optic nerve injury. (A) Schematic showing the schedule for dosing HR97-SunitiGel (5 µL of 1 mg/mL equivalent sunitinib concentration) relative to the timing of the optic nerve head (ONH) crush procedure. Brown Norway rats were dosed daily for 7 days and the ONH was crushed on day 0, 7, or 21 after the last dose. After 7 days, the retinas were harvested and stained with DAPI (blue) and RBPMs (red) for RGC counting. (B) Representative images with RGCs identified by the cell counting program outlined with green bounding boxes. Scale bar = 50 µm. (C) HR97-SunitiGel provided significant neuroprotective effects for up to 2 weeks after the last dose, with the effect waning after 4 weeks. Data are presented as mean  $\pm$  SD ( $n = 9\text{--}12$  per group), \* $p < 0.05$ . (D) SunitiGel provided neuroprotection for up to 1 week after the last dose with the effect waning after 2 weeks. The dotted line represents the mean RGC density in the Sham group. Data are presented as mean  $\pm$  SD ( $n = 5\text{--}12$  per group), \* $p < 0.05$  compared to the sham group, # $p < 0.05$  compared to SunitiGel. (For interpretation of the references to colour in this figure legend, the reader is referred to the web version of this article.)

sunitinib in the rabbit retina were comparable to concentrations found to be protective in the optic nerve crush model in rats. [6].

#### 4. Discussion

Patient adherence is important in treatment of chronic ocular diseases such as glaucoma, wherein patients must chronically apply IOP lowering eye drops. Typically, only 40%–75% of patients adhere to glaucoma drop therapy regimens, even in scenarios where the patients know they are being monitored and were provided free medication [16–18]. Failure to use medications as prescribed contributes to the progression of disease and can potentially lead to vision loss. Here, we investigate a complementary strategy to IOP lowering, which is to directly target survival of the RGCs independent of IOP [4,5]. In this scenario, there is an added challenge of achieving effective drug delivery

to the posterior segment with an eye drop, which is limited by ocular tissue barriers and uveal clearance [17,19,20]. Designing a drug delivery system that can effectively deliver drugs to the posterior segment for neuroprotection, utilizing a non-invasive administration approach, and providing prolonged therapeutic effect to reduce dosing frequency may address several unmet needs in glaucoma management.

Melanin is a biopolymer that resides within melanosomes in pigmented ocular tissues, such as the retinal pigment epithelium (RPE), choroid, iris, and ciliary body [7,21]. Melanin can be further classified as eumelanin and pheomelanin. Though the amount of pheomelanin in the eye is more variable in different populations, the amount of eumelanin in the RPE, pigmented ciliary epithelium, and iris pigment epithelium is relatively consistent regardless of skin and eye pigmentation [7]. There is an increasing amount of evidence indicating that binding to ocular melanin could affect the intraocular distribution and

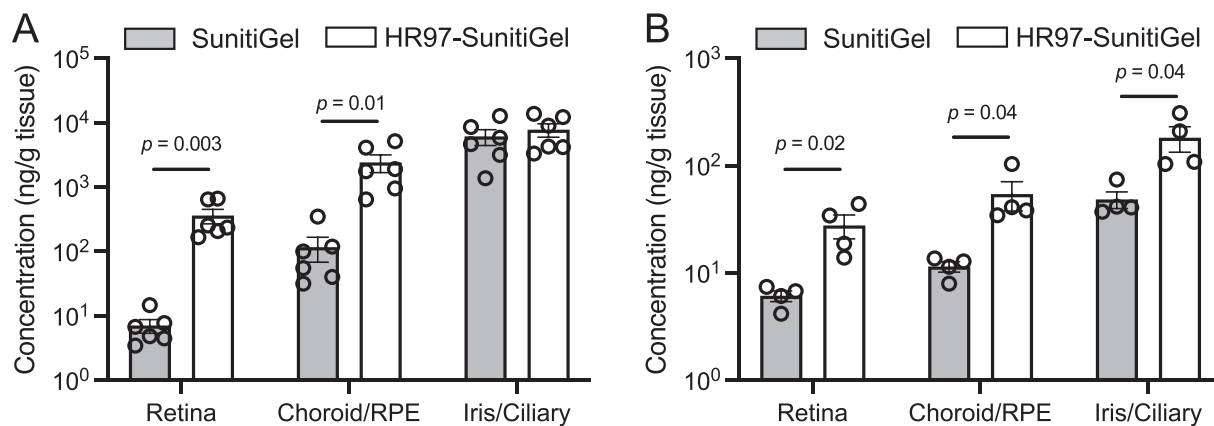


**Fig. 5.** Characterization of intraocular drug concentrations after topical dosing with SunitiGel or HR97-SunitiGel in rats and rabbits. (A) Brown Norway rats were dosed unilaterally with SunitiGel or HR97-SunitiGel once daily for 7 days, and ocular tissues were collected 14 days after the last dose (consistent with the 2-week dosing regimen shown in Fig. 4A). Combined levels of sunitinib and N-desethyl sunitinib were reported per tissue sample. Data are presented as mean  $\pm$  SEM ( $n = 6$  per group). (B) Dutch Belted rabbits were dosed unilaterally with SunitiGel or HR97-SunitiGel once daily for 7 days, and ocular tissues were collected 2 h after the last dose. Combined levels of sunitinib and N-desethyl sunitinib were reported per tissue sample. Data are presented as mean  $\pm$  SEM ( $n = 4$  per group). (For interpretation of the references to colour in this figure legend, the reader is referred to the web version of this article.)

pharmacodynamics of small molecule drugs. For example, studies have shown that in pigmented rabbits atropine had prolonged residence time [22], and pilocarpine induced a sustained miotic response [23]. Further, drug-melanin interactions and the amount of free *versus* melanin-bound drug have been characterized in retinal pigment epithelium cells [7,24–26], so have the correlation between *in vitro* cell uptake and *in vivo* intraocular pharmacokinetics [9,27]. Additionally, machine learning models have been applied to melanin binding data comprised of 3400 small molecule drugs to predict how structural properties impact melanin binding [9].

Cell-penetrating peptides, including TAT, penetratin, and polyarginine (R6 or R8), have been utilized for delivering drugs to the anterior or posterior segments of the eye [28–32]. In a recent study, researchers developed a novel peptide-dexamethasone conjugate composed of a cell-penetrating peptide, an enzyme-cleavable linker, and dexamethasone conjugated via a hydrazone bond. Following intravitreal injection, the conjugate remained stable in the vitreous, and the dexamethasone was released *via* intracellular interaction with cathepsin D, thus offering a distinctive approach for sustained drug delivery to the posterior segment of the eye [32]. In our previous work, we leveraged a super learning-based methodology to engineer multifunctional peptides that are cell-penetrating, melanin binding, and have low cytotoxicity [10]. We demonstrated that conjugating the IOP lowering drug, brimonidine tartrate, to an engineered multifunctional peptide (HR97) significantly increased the IOP lowering efficacy for up to 18 days, with a 17-fold increased area under the curve compared to brimonidine solution after a single intracameral injection in rabbits [10]. We also showed that SunitiGel effectively protected RGCs in the rat optic nerve head crush model with once weekly dosing with no evidence of toxicity in healthy eyes [6]. Here, by conjugating HR97 peptide to sunitinib, topical delivery of HR97-SunitiGel effectively protected RGCs for at least 2 weeks after the last topical dose.

RGC identification and quantification are often employed in studies investigating cell and vision loss in glaucoma [4,5,33,34]. The cell quantification has often been conducted manually by masked individuals hand-counting the cells [5,6] or using the Image J software [35,36]. Recently, the open-source CellProfiler and CellProfiler Analyst have received considerable attention for quantification of the cells because of its user-friendly interface, flexible analysis module, and integration of machine learning algorithms [37,38]. Although CellProfiler provides an automatic pipeline for quantifying cells, the accuracy is heavily reliant on image quality. Commercial software, such as Metamorph (BioVision, Waltham, MA), Cellomics (Thermo Fisher), or TruAI

deep-learning technology (Olympus) provide a convenient user interface and pre-designed modules to process and quantify cell images, but with annual subscription fees. The RGC quantifier developed in this study is based on the open source TensorFlow deep learning object detection system with the Faster R-CNN model. Although the model was trained on a relatively small image set, our cell counting program provided a high accuracy with increased flexibility to detect cells in images with varying cell densities and image qualities. Moreover, the model could be further trained with more confocal images in the future to accommodate different RGC staining qualities or expand to various systems of glaucoma animal models *via* transfer learning.

Although promising, our study is not without limitations. Previously, the cell culture model system highlighted the increase in uptake and retention provided by the HR97 peptide *in vitro* [10], yet the effects were less prominent here with a drug that is intrinsically melanin binding. Similarly, the *in vitro* melanin binding assay showed significant but relatively minor increases in melanin binding capacity and affinity. However, the increased melanin binding capacity of the HR97-sunitinib conjugate paired with the increased potential for cell-penetration did sustain the pharmacokinetic and pharmacodynamic effects of sunitinib in the ONH rat model *in vivo*. Though the pharmacokinetic analysis revealed higher sunitinib concentrations in the ocular tissues of rats than in rabbits, the sunitinib concentrations achieved in the retina of rabbits with topical HR97-SunitiGel dosing were similar to what was previously found to be efficacious in the rat ONH crush model [6]. The data support the frequently described phenomenon that rodent models are not sufficient for predicting drug delivery to the posterior segment with topical eye drops, and that confirmation in larger species is necessary [3]. Further, the choice of a cathepsin-labile linker was based on the fact that cathepsins are mainly found intracellularly, and they are only present in minute quantities in extracellular fluids such as vitreous and aqueous humor [39–42]. However, characterization of the linker cleavage and sunitinib release rate in cells and potential refinement of the linker chemistry may further prolong the therapeutic effect. Additionally, though we did demonstrate delivery of therapeutically relevant drug concentrations in rabbits, therapeutic efficacy has yet to be confirmed. Further, confirming the potential sustained therapeutic effects of the loading dosing approach followed by the intermittent dosing regimen (*e.g.*, once daily dosing for seven days followed by dosing once every 2 weeks) should be confirmed in large animals. Similarly, though we did not see any evidence of toxicity with intracameral injections of HR97-brimonidine and HR97 alone in rabbits [10], more thorough studies of intraocular biocompatibility would be an important next step in the

development of HR97-SunitiGel. The intrinsic melanin binding capacity of sunitinib limited the potential margin of benefit that could be observed for the duration of therapeutic effect provided by the HR97 conjugation, though we anticipate that more drastic improvements may be achievable for other drugs with low intrinsic melanin binding.

## 5. Conclusion

The development of innovative drug delivery systems that can overcome ocular barriers and enhance drug retention in the eye is essential for successful treatment of posterior segment diseases. Our study demonstrated that the HR97-sunitinib conjugate delivered via gel-forming eye drops (HR97-SunitiGel) provided increased sunitinib delivery to the posterior segment of rats and rabbits and prolonged neuroprotective effect for up to two weeks after the last dose in rats. Overall, the results obtained here demonstrate the benefits of increasing the melanin binding and cell penetration of small molecule drugs in the eye. The potential for developing topical eye drop delivery systems that can not only provide effective drug delivery to the posterior segment of the eye, but also require less frequent application, would be of high value clinically and in improving patient quality of life.

## CRediT authorship contribution statement

**Henry T. Hsueh:** Conceptualization, Data curation, Formal analysis, Funding acquisition, Investigation, Methodology, Project administration, Resources, Software, Validation, Visualization, Writing – original draft, Writing – review & editing. **Renee Ti Chou:** Conceptualization, Data curation, Formal analysis, Funding acquisition, Investigation, Methodology, Project administration, Resources, Software, Validation, Visualization, Writing – original draft, Writing – review & editing. **Usha Rai:** Data curation, Formal analysis, Investigation, Methodology, Writing – original draft. **Patricia Kolodziejski:** Data curation, Formal analysis, Methodology, Resources, Validation, Visualization, Writing – original draft, Writing – review & editing. **Wathsala Liyanage:** Conceptualization, Data curation, Formal analysis, Investigation, Methodology, Resources, Software, Validation, Visualization, Writing – original draft, Writing – review & editing. **Jahnavi Pejavar:** Data curation, Formal analysis, Investigation, Methodology, Validation, Visualization. **Ann Mozer:** Data curation, Formal analysis, Investigation, Methodology, Validation, Visualization, Writing – original draft. **Charlotte Davison:** Data curation, Formal analysis, Investigation, Methodology, Validation, Visualization, Writing – original draft. **Matthew B. Appell:** Data curation, Formal analysis, Methodology. **Yoo Chun Kim:** Conceptualization, Data curation, Formal analysis, Investigation, Methodology, Validation, Visualization, Writing – original draft. **Kirby T. Leo:** Data curation, Formal analysis, Investigation, Methodology, Validation, Visualization, Writing – original draft. **Hyeyoung Kwon:** Data curation, Formal analysis, Investigation, Methodology, Visualization, Writing – original draft. **Maanasa Sista:** Data curation, Formal analysis, Investigation, Methodology, Validation, Writing – original draft. **Nicole M. Anders:** Data curation, Formal analysis. **Avelina Hemingway:** Data curation, Formal analysis. **Sri Vishnu Kiran Rompicharla:** Methodology. **Ian Pitha:** Conceptualization, Data curation, Formal analysis, Investigation, Methodology, Supervision, Validation, Visualization, Writing – original draft. **Donald J. Zack:** Conceptualization, Project administration, Resources. **Justin Hanes:** Conceptualization, Investigation, Resources, Supervision. **Michael P. Cummings:** Conceptualization, Data curation, Formal analysis, Investigation, Methodology, Supervision, Visualization, Writing – original draft, Writing – review & editing. **Laura M. Ensign:** Conceptualization, Data curation, Formal analysis, Funding acquisition, Investigation, Methodology, Project administration, Resources, Software, Supervision, Validation, Visualization, Writing – original draft, Writing – review & editing.

## Declaration of Competing Interest

H.T.H., R.T.C., J.H., M.P.C. and L.M.E. are named as inventors on a provisional patent related to the presented research work that was jointly filed by Johns Hopkins University and the University of Maryland, College Park. H.T.H., L.M.E., and J.H. are named as inventors on a family of patents describing the gel-forming eye drop technology used in this work, and are co-founders of Novus Vision, LLC, a start-up company developing the gel-forming eye drop technology. D.J.Z. is an inventor on patents related to sunitinib and neuroprotection. Some of these patents have been licensed to Graybug Vision and to Perceive Biotherapeutics. D.J.Z. is a co-founder and equity owner in Perceive Biotherapeutics. The terms of this arrangement are being managed by the Johns Hopkins University in accordance with its conflict-of-interest policies. The other authors declare no competing interests.

## Data availability

Data will be made available on request.

## Acknowledgements

We are very grateful for the veterinary and husbandry staff for their assistance, especially Sherrie Hawkes and Darlene Kyler. We thank Fareeha Zulfiqar for ordering and organizing the materials and equipment. We appreciate Mary Ellen Pease, Rhonda Grebe, and Arina Korneva for assisting and optimizing LSM 710 confocal microscope and TEM protocols. We thank Malia Edwards for obtaining the human donor eyes for research purpose. We acknowledge and appreciate input from Daiqin Chen regarding the traceless linker design and optimization from the original protocols. This work was supported by the National Institutes of Health (NIH) (grant nos. R01EY026578 and R01EY031041), the Robert H. Smith Family Foundation, Marcella E. Woll and the Maryland E-Nnovation Initiative Fund (MEIF) to establish the Marcella E. Woll Professorship in Ophthalmology, and Research to Prevent Blindness. H.T.H. was supported in part by a National Eye Institute Training Grant (T32EY007143). R.T.C. was supported in part by a National Science Foundation Award (DGE-1632976). Drug measurements were conducted by the Analytical Pharmacology Core (APC) of the Sidney Kimmel Comprehensive Cancer Center at Johns Hopkins. The work conducted by the APC was supported by the NIH (grant nos. P30CA006973 and S10OD020091) and the National Center for Advancing Translational Sciences (NCATS) (grant no. UL1TR001079), a component of the NIH, and the NIH Roadmap for Medical Research. The research contents are solely the responsibility of the authors and do not necessarily represent the official view of the NCATS or the NIH.

## Appendix A. Supplementary data

Supplementary data to this article can be found online at <https://doi.org/10.1016/j.jconrel.2023.08.058>.

## References

- [1] A.P. Tse, et al., Glaucoma treatment adherence at a United Kingdom general practice, *Eye (Lond)* 30 (8) (2016) 1118–1122.
- [2] A. Chawla, J.N. McGaillard, M. Batterbury, Use of eyedrops in glaucoma: how can we help to reduce non-compliance? *Acta Ophthalmol. Scand.* 85 (4) (2007) 464.
- [3] Y.C. Kim, et al., Gelling hypotonic polymer solution for extended topical drug delivery to the eye, *Nat. Biomed. Eng.* 4 (11) (2020) 1053–1062.
- [4] D.S. Welsbie, et al., Functional genomic screening identifies dual leucine zipper kinase as a key mediator of retinal ganglion cell death, *Proc. Natl. Acad. Sci. U. S. A.* 110 (10) (2013) 4045–4050.
- [5] D.S. Welsbie, et al., Enhanced functional genomic screening identifies novel mediators of dual leucine zipper kinase-dependent injury signaling in neurons, *Neuron* 94 (6) (2017) 1142–1154 e6.
- [6] Y.C. Kim, et al., A hypotonic gel-forming eye drop provides enhanced intraocular delivery of a kinase inhibitor with melanin-binding properties for sustained protection of retinal ganglion cells, *Drug Deliv. Transl. Res.* 12 (4) (2022) 826–837.

- [7] A.K. Rimpela, et al., Melanin targeting for intracellular drug delivery: quantification of bound and free drug in retinal pigment epithelial cells, *J. Control. Release* 283 (2018) 261–268.
- [8] A.K. Rimpela, et al., Implications of melanin binding in ocular drug delivery, *Adv. Drug Deliv. Rev.* 126 (2018) 23–43.
- [9] P. Jakubiak, et al., Understanding molecular drivers of melanin binding to support rational design of small molecule ophthalmic drugs, *J. Med. Chem.* 61 (22) (2018) 10106–10115.
- [10] H.T. Hsueh, et al., Machine learning-driven multifunctional peptide engineering for sustained ocular drug delivery, *Nat. Commun.* 14 (2023) 2509.
- [11] L.R. Staben, et al., Targeted drug delivery through the traceless release of tertiary and heteroaryl amines from antibody-drug conjugates, *Nat. Chem.* 8 (12) (2016) 1112–1119.
- [12] N.P. Cheruvu, A.C. Amrite, U.B. Kompella, Effect of eye pigmentation on transscleral drug delivery, *Investig. Ophthalmol. Vis. Sci.* 49 (1) (2008) 333–341.
- [13] H.T. Hsueh, et al., Ion-complex microcrystal formulation provides sustained delivery of a multimodal kinase inhibitor from the subconjunctival space for protection of retinal ganglion cells, *Pharmaceutics* 13 (5) (2021).
- [14] L. Liu, et al., Deep learning for generic object detection: a survey, *Int. J. Comput. Vis.* 128 (2) (2020) 261–318.
- [15] S. Ren, K. He, R. Girshick, J. Sun, Faster R-CNN: towards real-time object detection with region proposal networks, *Adv. Neural Inf. Proces. Syst.* 28 (2015).
- [16] B.L. Nordstrom, et al., Persistence and adherence with topical glaucoma therapy, *Am J. Ophthalmol.* 140 (4) (2005) 598–606.
- [17] C.O. Okeke, et al., Interventions improve poor adherence with once daily glaucoma medications in electronically monitored patients, *Ophthalmology* 116 (12) (2009) 2286–2293.
- [18] C.O. Okeke, et al., Adherence with topical glaucoma medication monitored electronically the Travatan dosing aid study, *Ophthalmology* 116 (2) (2009) 191–199.
- [19] G.A. Rodrigues, et al., Topical drug delivery to the posterior segment of the eye: addressing the challenge of preclinical to clinical translation, *Pharm. Res.* 35 (12) (2018) 245.
- [20] R. Singh, et al., Clinical evaluation of pazopanib eye drops in healthy subjects and in subjects with neovascular age-related macular degeneration, *Retina* 34 (9) (2014) 1787–1795.
- [21] D.N. Hu, J.D. Simon, T. Sarna, Role of ocular melanin in ophthalmic physiology and pathology, *Photochem. Photobiol.* 84 (3) (2008) 639–644.
- [22] M. Salazar, K. Shimada, P.N. Patil, Iris pigmentation and atropine mydriasis, *J. Pharmacol. Exp. Ther.* 197 (1) (1976) 79–88.
- [23] A. Urtti, et al., Effect of ocular pigmentation on pilocarpine pharmacology in the rabbit eye. II. Drug response, *Int. J. Pharm.* 19 (1) (1984) 53–61.
- [24] S. Bahrpeyma, et al., Mechanisms of cellular retention of melanin bound drugs: experiments and computational modeling, *J. Control. Release* 348 (2022) 760–770.
- [25] A.K. Rimpela, et al., Drug distribution to retinal pigment epithelium: studies on melanin binding, cellular kinetics, and single photon emission computed tomography/computed tomography imaging, *Mol. Pharm.* 13 (9) (2016) 2977–2986.
- [26] L. Hellinen, et al., Characterization of artificially re-pigmented ARPE-19 retinal pigment epithelial cell model, *Sci. Rep.* 9 (1) (2019) 13761.
- [27] P. Jakubiak, et al., Establishment of an in vitro-in vivo correlation for melanin binding and the extension of the ocular half-life of small-molecule drugs, *Mol. Pharm.* 16 (12) (2019) 4890–4901.
- [28] L.N. Johnson, S.M. Cashman, R. Kumar-Singh, Cell-penetrating peptide for enhanced delivery of nucleic acids and drugs to ocular tissues including retina and cornea, *Mol. Ther.* 16 (1) (2008) 107–114.
- [29] G.G. Jose, et al., A cationic peptide, TAT-Cd degrees, inhibits herpes simplex virus type 1 ocular infection in vivo, *Invest. Ophthalmol. Vis. Sci.* 54 (2) (2013) 1070–1079.
- [30] F. de Cogan, et al., Topical delivery of anti-VEGF drugs to the ocular posterior segment using cell-penetrating peptides, *Invest. Ophthalmol. Vis. Sci.* 58 (5) (2017) 2578–2590.
- [31] S. Pescina, et al., Cell penetrating peptides in ocular drug delivery: state of the art, *J. Control. Release* 284 (2018) 84–102.
- [32] M. Bhattacharya, et al., Release of functional dexamethasone by intracellular enzymes: a modular peptide-based strategy for ocular drug delivery, *J. Control. Release* 327 (2020) 584–594.
- [33] M.E. Pease, et al., Effect of CNTF on retinal ganglion cell survival in experimental glaucoma, *Investig. Ophthalmol. Vis. Sci.* 50 (5) (2009) 2194–2200.
- [34] R.S. Harwerth, J.L. Wheat, N.V. Rangaswamy, Age-related losses of retinal ganglion cells and axons, *Invest. Ophthalmol. Vis. Sci.* 49 (10) (2008) 4437–4443.
- [35] J.B. Sheffeld, ImageJ, a useful tool for biological image processing and analysis, *Microsc. Microanal.* 13 (S02) (2007) 200–201.
- [36] M.D. Abràmoff, P.J. Magalhães, S.J. Ram, Image processing with ImageJ, *Biophoton. Int.* 11 (7) (2004) 36–42.
- [37] A.C. Dordea, et al., An open-source computational tool to automatically quantify immunolabeled retinal ganglion cells, *Exp. Eye Res.* 147 (2016) 50–56.
- [38] A.E. Carpenter, et al., CellProfiler: image analysis software for identifying and quantifying cell phenotypes, *Genome Biol.* 7 (10) (2006) R100.
- [39] J. Wasselinus, et al., Cathepsin B in the rat eye, *Graefes Arch. Clin. Exp. Ophthalmol.* 241 (11) (2003) 934–942.
- [40] H. Appelqvist, et al., The lysosome: from waste bag to potential therapeutic target, *J. Mol. Cell Biol.* 5 (4) (2013) 214–226.
- [41] P.E. Rakoczy, et al., Distribution of cathepsin D in human eyes with or without age-related maculopathy, *Exp. Eye Res.* 69 (4) (1999) 367–374.
- [42] M. Goel, et al., Aqueous humor dynamics: a review, *Open Ophthalmol. J.* 4 (2010) 52–59.